Inorganic Chemistry

ARTICLE

pubs.acs.org/IC

Oxidation State Analysis of a Four-Component Redox Series $[Os(pap)_2(Q)]^n$ Involving Two Different Non-Innocent Ligands on a Redox-Active Transition Metal

Dipanwita Das,[†] Biprajit Sarkar,[‡] Tapan Kumar Mondal,[§] Shaikh M. Mobin,[†] Jan Fiedler,[∥] Wolfgang Kaim,*[,‡] and Goutam Kumar Lahiri*[,†]

[†]Department of Chemistry, Indian Institute of Technology Bombay, Powai, Mumbai-400076, India

[‡]Institut für Anorganische Chemie, Universität Stuttgart, Pfaffenwaldring 55, D-70550 Stuttgart, Germany

[§]Department of Chemistry, Jadavpur University, Jadavpur, Kolkata-700032, India

[∥]J. Heyrovský Institute of Physical Chemistry, v.v.i., Academy of Sciences of the Czech Republic, Dolejškova 3, CZ-18223 Prague, Czech Republic

Supporting Information

ABSTRACT: Complexes $[Os(pap)_2(Q)]$ (**1**−**4**) have been obtained and structurally characterized for pap = 2-phenylazopyridine and Q = 4,6-di-*tert*-butyl-*N*-aryl-*o*-iminobenzoquinone (aryl = phenyl (**1**), 3,5-dichlorophenyl (**2**), 3,5-dimethoxyphenyl (**3**), or 3,5-di-*tert*-butylphenyl (**4**)). The oxidized form $(\mathbf{3})(ClO_4)_2$ was also crystallographically characterized while the odd-electron intermediates $[Os(pap)_2(Q)]^+$ ($\mathbf{1}^+$−$\mathbf{4}^+$) and $[Os(pap)_2(Q)]^-$ ($\mathbf{2}^-$) were investigated by electron paramagnetic resonance (EPR) and UV−vis−NIR spectroelectrochemistry in conjunction with density functional theory (DFT) spin density and time-dependent DFT (TD-DFT) calculations. The results from the structural, spectroscopic, and electrochemical experiments and from the computational studies allow for the assignments $[Os^{II}(pap^0)_2(Q^0)]^{2+}$, $[Os^{II}(pap^0)_2(Q^{\bullet-})]^+$, $[Os^{IV}(pap^{\bullet-})_2(Q^{2-})]$, and $[Os^{II}(pap^{\bullet-})(pap^0)(Q^{2-})]^-$, with comproportionation constants $K_c \approx 10^{3.5}$, 10^{10}, 10^{18}, and 10^5, respectively. The redox potentials and the comproportionation constants exhibit similarities and differences between Ru and Os analogues. While the Q-based redox reactions show identical potentials, the more metal-involving processes exhibit cathodic shifts for the osmium systems, leading to distinctly different comproportionation constants for some intermediates, especially to a stabilization of the neutral osmium compounds described in this article. The example $[Os(pap)_2(Q)]^n$ illustrates especially the power of combined structural and EPR analysis with support from DFT towards the valence state description of transition metal complexes incorporating redox non-innocent ligands.

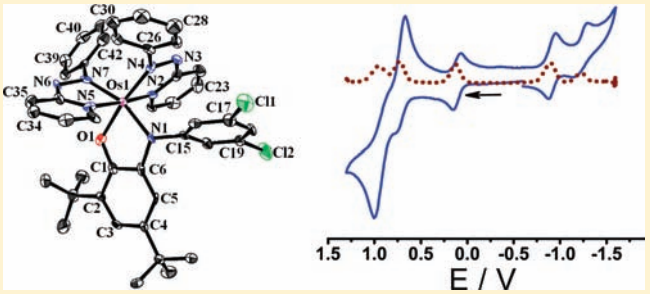

1. INTRODUCTION

The concept of redox-active or "non-innocent" ligands in transition metal complexes has not only become more popular in recent years, it has also been extended to systems with more than one metal and/or more than one (equivalent or nonequivalent) such ligand.[1] The occurrence of the latter entities in the biological context of enzymatic catalysis, involving, for example, non-innocent coenzyme ligands and a non-innocent substrate coordinated to a transition metal,[2] has prompted us to develop model compounds in which a transition metal binds two non-innocently behaving ligands such as porphyrins, quinone-type compounds, or NO within three-component redox series.[3] Extending this pattern to *three* partially nonequivalent redox-active ligands and thus to a four-component system, we have now combined a series of quinonoid ligands Q^1-Q^4 from the well-established[4] group of 4,6-di-*tert*-butyl-*N*-aryl-*o*-iminobenzoquinones, Q, with two well reducible[5] azo-containing 2-phenylazopyridine (pap) chelate ligands at the heavy homologue of iron, osmium, with its wide range of accessible oxidation states (Scheme 1).

The use of the two different but energetically not too much separated π acceptor ligands pap and Q was based on the bidentate chelate binding ability with concomitant stabilization of complexes, and on the well established structural manifestations of the oxidation states of these redox-active ligands, for example, the lengthening of the azo bond in pap and related molecules[5,6] on reduction, and the decreasing C−C bond alternancy on reduction of quinones.[7]

Both the quinonoid systems, Q, and the azo-containing ligands, pap, in $[Os(pap)_2(Q)]^n$ are thus well-defined regarding their oxidation states through metrical parameters from high-quality X-ray diffraction.[4−7] In addition to these structural experiments

Received: March 25, 2011
Published: June 23, 2011

the accessible members of the redox series $[Os(pap)_2(Q)]^n$ ($\mathbf{1}^n$−$\mathbf{4}^n$) will be characterized and analyzed by cyclic voltammetry, differential pulse voltammetry, electron paramagnetic resonance (EPR), and UV−vis−NIR spectroelectrochemistry in conjunction with density functional theory (DFT) spin density and time-dependent DFT (TD-DFT) calculations; the comparison with the ruthenium analogues[8] will also be made.

2. EXPERIMENTAL SECTION

The precursor complex *cis-trans-cis*-$Os(pap)_2(Cl)_2$[9] and the substituted 2-anilino-4,6-di-*tert*-butylphenol (H_2Q)[10] were prepared according to the reported procedures. Other chemicals and solvents were of reagent grade and used as received. For spectroscopic and electrochemical studies HPLC grade solvents were used.

Instrumentation. UV−vis−NIR spectroelectrochemical studies were performed in CH_2Cl_2/0.1 M $[Bu_4N][PF_6]$ at 298 K using an optically transparent thin layer electrode (OTTLE)[11] cell mounted in the sample compartment of a J&M TIDAS spectrophotometer. The EPR measurements were made in a two-electrode capillary tube[12] with an X-band (9.5 GHz) Bruker system ESP300 spectrometer. ^{1}H NMR spectra were obtained with a 300 MHz Varian spectrometer. Cyclic voltammetric and differential pulse voltammetric measurements were carried out using a PAR model 273A electrochemistry system. Platinum wire working and auxiliary electrodes and an aqueous saturated calomel reference electrode (SCE) were used in a three-electrode configuration. The supporting electrolyte was 0.1 M $[Et_4N][ClO_4]$, and the solute concentration was about 10^{-3} M. The half-wave potential $E°_{298}$ was set equal to $0.5(E_{pa} + E_{pc})$, where E_{pa} and E_{pc} are anodic and cathodic cyclic voltammetric peak potentials, respectively. Elemental analyses were carried out with a Perkin-Elmer 240C elemental analyzer. Electrospray mass spectra were recorded on a Micromass Q-ToF mass spectrometer.

Scheme 1

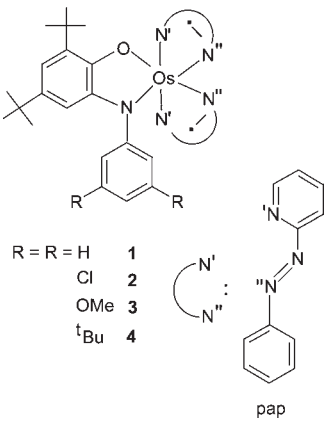

Preparation of Complexes. The complexes were prepared by following a similar synthetic protocol; a representative method is described for complex **1**.

*[Os(pap)$_2$(Q^1)], (**1**).* Initially the starting material *cis-trans-cis*-$Os(pap)_2(Cl)_2$ (50 mg, 0.079 mmol) was taken in a 20 mL 1:1 mixture of ethanol and water and was refluxed for 5 min under dinitrogen atmosphere. To this, the ligand 2-anilino-4,6-di-*tert*-butylphenol (H_2Q^1) (36 mg, 0.119 mmol) and a few drops of NEt_3 were added, and the mixture was refluxed for 72 h to yield a dark brown suspension. The microcrystalline brown solid was collected by filtration and air-dried. The precipitate was then purified by column chromatography using a silica gel column (60−120 mesh). The brown band of **1** was eluted by CH_2Cl_2. On removal of the solvent under reduced pressure the pure complex **1** was obtained as a dark solid which was further dried under vacuum.

1: Yield, 50 mg (74%). $C_{42}H_{43}N_7OOs$ Anal. Calcd (Found): C, 59.06 (59.20); H, 5.08 (5.17); N, 11.49 (11.31). ESI MS (in CH_2Cl_2): *m/z* Calcd (Found) for $[\mathbf{1}]^+$: 853.31 (853.62). ^{1}H NMR in $CDCl_3$ (δ, ppm(*J*, Hz)): 7.84 (d, 1H, 8.7), 7.48(d, 1H, 7.8), 7.21 (m, 6H), 7.11 (t, 2H, 7.2, 7.5), 7.05 (m, 4H), 6.85 (t, 2H, 7.2, 7.5), 6.67 (d, 4H, 8.1), 6.41 (s, 2H), 6.35 (d, 2H, 7.8), 6.24 (t, 1H, 6.0, 6.0), 1.56(s, 9H), 1.41 (s, 9H).

Table 1. Selected Crystallographic Data for 1, 2, 3, 4, and $(3)(ClO_4)_2$

	1	2	3	4	$(3)(ClO_4)_2$
mol formula	$C_{42}H_{43}N_7OOs$	$C_{42}H_{41}Cl_2N_7OOs$	$C_{44}H_{47}N_7O_3Os$	$C_{50}H_{59}N_7OOs$	$C_{44}H_{47}Cl_2N_7O_{11}Os$
Fw	852.03	920.92	912.09	964.24	1110.99
cryst sym	orthorhombic	orthorhombic	monoclinic	monoclinic	triclinic
space group	*P*21 21 21	*P*21 21 21	*P*21/*c*	*P*21/*c*	$P\bar{1}$
a (Å)	12.0254(14)	12.5063(13)	15.089(7)	24.1605(16)	12.6086(3)
b (Å)	15.2317(13)	15.3816(14)	11.707(7)	13.2360(11)	13.6633(3)
c (Å)	20.5384(19)	20.364(2)	22.652(10)	30.241(2)	14.9412(4)
α (deg)	90	90	90	90	76.683(2)
β (deg)	90	90	93.94(4)	110.005(8)	78.805(2)
γ (deg)	90	90	90	90	67.856(2)
V (Å^3)	3762.0(6)	3917.3(7)	3992(3)	9087.3(12)	2303.52(10)
Z	4	4	4	8	2
μ (mm^{-1})	3.432	3.434	3.244	2.851	2.951
T (K)	120(2)	120(2)	120(2)	120(2)	150(2)
D_{calcd} (g cm^{-3})	1.504	1.561	1.518	1.410	1.602
F (000)	1712	1840	1840	3936	1116
2*θ* range(deg)	2.93 to 24.99	3.11 to 27.50	3.15 to 25.00	2.97 to 25.00	2.99 to 32.75
data/restraints/parameters	6617/0/466	8974/318/484	7006/0/504	8004/0/544	15127/0/631
R1, wR2 [$I > 2\sigma(I)$]	0.0313, 0.0442	0.0380, 0.0430	0.0452, 0.0862	0.0227, 0.0493	0.0508, 0.1091
R1, wR2(all data)	0.0458, 0.0457	0.0699, 0.0466	0.0850, 0.0913	0.0327, 0.0505	0.0857, 0.1144
GOF	0.787	0.608	0.910	0.927	0.971
largest diff. peak/hole, (e Å^{-3})	1.141 and −0.834	2.393 and −1.151	1.454 and −1.049	1.077 and −0.593	1.925 and −1.204

dx.doi.org/10.1021/ic200615s |*Inorg. Chem.* 2011, 50, 7090–7098

Table 2. Experimental (X-ray) and DFT Calculated Selected Bond Distances (Å)

	1		2	3	4	$(3)(ClO_4)_2$
bond distances	X-ray	DFT	X-ray	X-ray	X-ray	X-ray
Os(1)−O(1)	2.034(4)	2.063	2.021(4)	2.026(5)	2.037(2)	2.024(3)
Os(1)−N(1)	2.023(4)	2.048	2.020(4)	2.041(6)	2.007(2)	2.025(4)
Os(1)−N(2)	2.037(4)	2.037	2.023(4)	2.019(6)	2.007(2)	2.078(4)
Os(1)−N(4)	1.963(5)	1.997	1.962(4)	1.973(6)	1.975(2)	2.012(4)
Os(1)−N(5)	2.046(4)	2.057	2.019(4)	2.045(6)	2.044(2)	2.034(4)
Os(1)−N(7)	1.951(5)	2.003	1.947(4)	1.974(6)	1.983(2)	2.002(4)
C(1)−O(1)	1.326(6)	1.353	1.331(6)	1.352(8)	1.327(3)	1.285(6)
C(6)−N(1)	1.386(8)	1.390	1.404(7)	1.373(9)	1.387(4)	1.324(6)
N(3)−N(4)	1.327(5)	1.345	1.323(5)	1.355(7)	1.332(3)	1.288(5)
N(6)−N(7)	1.346(6)	1.355	1.333(6)	1.332(7)	1.341(3)	1.297(5)
C(1)−C(2)	1.432(7)	1.416	1.430(7)	1.417(10)	1.402(4)	1.427(6)
C(2)−C(3)	1.389(8)	1.398	1.403(8)	1.389(10)	1.376(4)	1.355(7)
C(3)−C(4)	1.420(7)	1.416	1.389(7)	1.406(10)	1.409(4)	1.444(7)
C(4)−C(5)	1.389(8)	1.392	1.377(7)	1.365(10)	1.375(4)	1.344(7)
C(5)−C(6)	1.418(8)	1.409	1.386(8)	1.388(10)	1.391(4)	1.426(7)
C(6)−C(1)	1.409(8)	1.419	1.428(7)	1.385(9)	1.423(4)	1.464(7)
C(15)−N(1)	1.425(8)	1.427	1.404(6)	1.416(8)	1.436(3)	1.445(6)

2: Yield, 55 mg (76%). $C_{42}H_{41}Cl_2N_7OOs$ Anal. Calcd (Found): C, 54.71 (54.63); H, 4.49 (4.52); N, 10.64 (10.53). ESI MS (in CH_2Cl_2): *m*/*z* Calcd (Found) for $[\mathbf{2}]^+$: 921.23 (921.50). ^{1}H NMR in $CDCl_3$ (δ, ppm(*J*, Hz)): 7.94 (d, 1H, 8.4), 7.50(d, 1H, 6.0), 7.36 (m, 2H), 7.19 (m, 3H), 7.00 (m, 4H), 6.83 (m, 3H), 6.67 (d, 2H, 8.1), 6.53 (m, 5H), 6.09 (s, 2H), 1.56(s, 9H), 1.37 (s, 9H).

3: Yield, 56 mg (77%). $C_{44}H_{47}N_7O_3Os$ Anal. Calcd (Found): C, 57.81 (57.53); H, 5.19 (5.14); N, 10.73 (10.82). ESI MS (in CH_2Cl_2): *m*/*z* Calcd (Found) for $[\mathbf{3}]^+$: 913.33 (913.70). ^{1}H NMR in $CDCl_3$ (δ, ppm(*J*, Hz)): 7.89 (d, 1H, 8.1), 7.50 (d, 1H, 5.7), 7.21 (m, 2H), 7.13 (t, 2H, 7.5, 7.2), 7.04 (m, 4H), 6.43 (d, 3H, 7.8), 6.26 (m, 4H), 6.00 (m, 2H), 5.85 (s, 4H), 3.70 (s, 6H),1.56(s, 9H), 1.41 (s, 9H).

4: Yield, 56 mg (73%). $C_{50}H_{59}N_7OOs$ Anal. Calcd. (Found): C, 62.15 (62.32); H, 6.16 (6.02); N, 10.15 (10.10). ESI MS (in CH_3CN): *m*/*z* Calcd (Found) for $[\mathbf{4}]^+$: 965.43 (965.80). ^{1}H NMR in $CDCl_3$ (δ, ppm(*J*, Hz)): 7.94 (d, 1H, 7.5), 7.54(d, 2H, 6.2), 7.20 (m, 2H), 7.09 (m, 3H), 6.99 (m, 4H), 6.58 (m, 4H), 6.39 (m, 2H), 6.22 (s, 2H), 6.10 (s, 1H), 5.90 (d, 2H, 7.5), 1.56(s, 9H), 1.45 (s, 9H), 1.42 (s, 18H).

$[Os(pap)_2(Q^3)](ClO_4)_2$, $(\mathbf{3})(ClO_4)_2$. Unlike **1**, **2**, and **4**, the complex **3** was partially oxidized to the $\mathbf{3}^{2+}$ state during the chromatographic purification process. Thus, the oxidized $\mathbf{3}^{2+}$ was eluted from the same column using a mixture of $HClO_4$ (0.05 mL) in CH_3OH (20 mL). The slow evaporation of the said solution yielded single crystals of $(\mathbf{3})(ClO_4)_2$ which have been characterized by X-ray diffraction and microanalytical analysis.

$(\mathbf{3})(ClO_4)_2$: Yield, 6 mg (7%). $C_{44}H_{47}Cl_2N_7O_{11}Os$ Anal. Calcd (Found): C, 47.51 (47.67); H, 4.26 (4.21); N, 8.82 (8.67). ESI MS (in CH_3CN): *m*/*z* Calcd (Found) for $\{(\mathbf{3})(ClO_4)\}^+$: 1012.28 (1012.74).

Crystallography. Single crystals of **1**−**4** and $(\mathbf{3})(ClO_4)_2$ were grown by slow evaporation of acetonitrile and methanol-$HClO_4$ (20:0.05) solutions, respectively. X-ray data for all complexes were collected using an OXFORD XCALIBUR-S CCD single crystal X-ray diffractometer. The structures were solved and refined by full-matrix least-squares techniques on F^2 using the SHELX-97 program.[13] The absorption corrections were done by multiscan (SHELXTL program package), and all the data were corrected for Lorentz, polarization effects. Hydrogen atoms were included in the refinement process as per the riding model. The molecule $[\mathbf{3}](ClO_4)_2$ contains one partially disordered ClO_4^- at the ratio of 53:47.

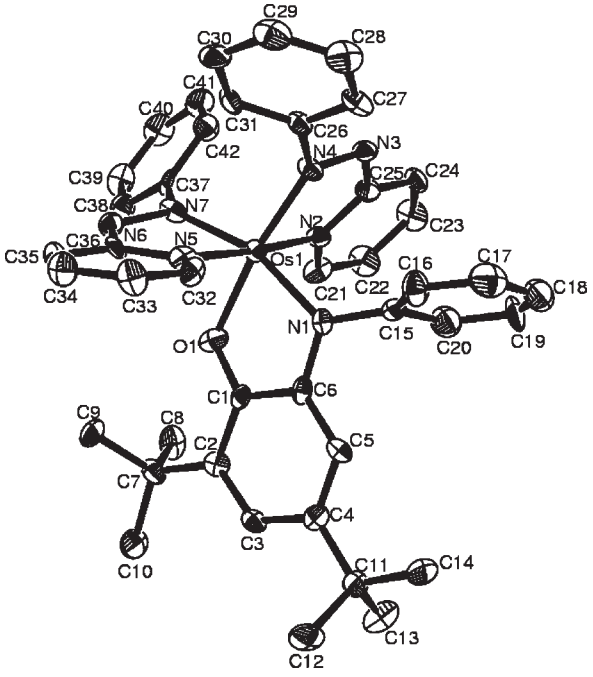

Figure 1. ORTEP diagram of **1**. Ellipsoids are drawn at 50% probability. Hydrogen atoms are omitted for clarity.

Computational Details. Full geometry optimizations were carried out using the DFT method at the (U)B3LYP for $\mathbf{1}^+$, $\mathbf{1}^-$ and (R)B3LYP level for $\mathbf{1}^{2+}$ and **1**.[14] All elements except osmium were assigned the 6-31G(d) basis set. The SDD basis set with effective core potential was employed for the osmium atom.[15] The vibrational frequency calculations were performed to ensure that the optimized geometries represent the local minima and there are only positive eigenvalues. All calculations were performed with the Gaussian03 program package.[16] Vertical electronic excitations based on B3LYP optimized geometries were computed for the TD-DFT[17] formalism in acetonitrile using the conductor-like

dx.doi.org/10.1021/ic200615s |*Inorg. Chem.* 2011, 50, 7090–7098

polarizable continuum model (CPCM).[18] GaussSum[19] was used to calculate the fractional contributions of various groups to each molecular orbital.

3. RESULTS AND DISCUSSION

Using the configurationally stable *ctc*-Os(pap)$_2$Cl$_2$[9] with *trans*-positioned pyridyl functions as starting material, we were able to isolate and crystallize the compounds **1**−**4** and (**3**)(ClO$_4$)$_2$. (*ctc* refers to the *cis* (*c*) or *trans* (*t*) positions of azo-N, pyridyl-N, and Cl or N/O).[9]

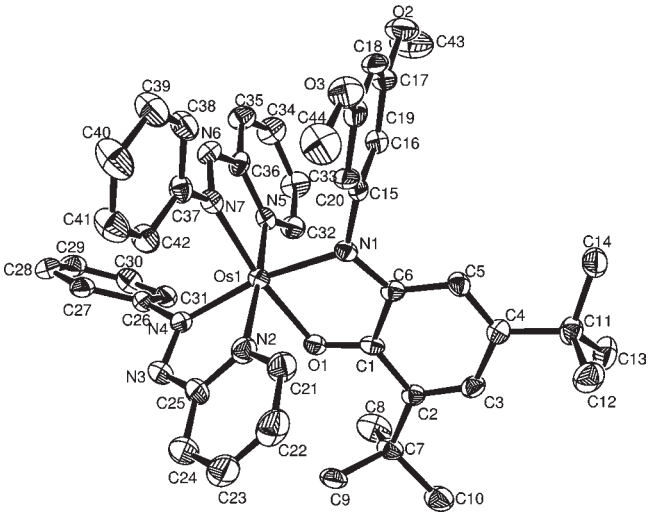

Figure 2. ORTEP diagram of the cationic part of (**3**)(ClO$_4$)$_2$. Ellipsoids are drawn at 50% probability. The counteranions (ClO$_4^-$) and hydrogen atoms are omitted for clarity.

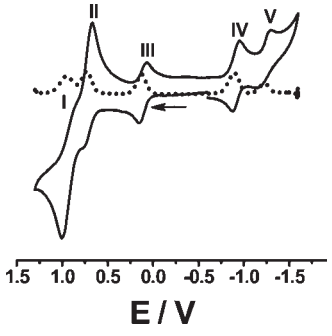

Figure 3. Cyclic voltammogram (solid lines) and differential pulse voltammogram (dashed lines) of **2** in CH$_2$Cl$_2$/0.1 M [Et$_4$N][ClO$_4$] versus SCE. Scan rate: 100 mV/s.

In addition to structural identification by X-ray diffraction (Tables 1, 2, Table S1, Figures 1, 2, Supporting Information, Figures S1−S3), the compounds were characterized by elemental analysis, mass spectrometry, and ^{1}H NMR spectroscopy (see Experimental Section). The latter revealed narrow resonance lines at the expected positions, that is, the absence of paramagnetic shifts.

According to the cyclic voltammetry and differential pulse voltammetry experiments (Figure 3, Table 3) the systems *ctc*-[Os(pap)$_2$(Q)]^n could be studied in four different complex charges (n = 2+,+,0,−) which will be discussed in the following step by step, with the help of structural and EPR information (Figures 4, 5, Table 4) as supported by DFT calculations (Figures 6−8, Supporting Information, Figure S4, Tables 2, 7, Supporting Information, Tables S1−S5). On the basis of these assignments, we will discuss the electronic absorption behavior in UV−vis−NIR spectroelectrochemistry (Supporting Information, Figures S5−S10, Table 5, 6, Supporting Information, Table S6−S8) in conjunction with an overall assessment of electronic structure changes.

***ctc*-[Os(pap)$_2$(Q)]$^{2+}$.** The dications could be generated spectroelectrochemically for all four systems; they exhibit a relatively small comproportionation constant $K_c = 10^3-10^4$ (comproportionation constant, $RT \ln K_c = nF(\Delta E)$).[8] One example, *ctc*-(**3**)(ClO$_4$)$_2$ could be crystallized for X-ray structure analysis (Figure 2, Tables 1, 2, Supporting Information, Table S1).

The structure analysis confirms the expected configuration with two kinds of unreduced acceptor ligands, pap and Q, bonded by the efficient π donor[20] metal osmium(II). Accordingly, a relatively long[5,6,21] N═N bond of 1.29 Å is observed for the pap ligands ((N═N)^0 < 1.30 Å, (N−N)$^{\bullet-}$ ≥ 1.33 Å, (N−N)$^{2-}$ ≥ 1.40 Å[5,6]) as is a pronounced alternancy of the C−C bonds in the coordinated iminoquinone Q with short C(2)−C(3) and C(4)−C(5) bonds in addition to short C═O and C═N distances (Table 2). The DFT calculations confirm this interpretation and reveal three low lying unoccupied orbitals, first an iminoquinone-centered π^* LUMO and then two close-lying pap-based second and third lowest unoccupied π^* MOs (Supporting Information, Tables S3, S7 and Figure 8).

***ctc*-[Os(pap)$_2$(Q)]$^+$.** In agreement with the preceding results from DFT calculations the one-electron reduction of *ctc*-[Os(pap)$_2$(Q)]$^{2+}$ (or one-electron oxidation of *ctc*-Os(pap)$_2$(Q)) leads to species *ctc*-[Os^{II}(pap^0)$_2$(Q$^{\bullet-}$)]$^+$ with *o*-iminobenzosemiquinone ligands. The K_c values for these intermediates are rather

Table 3. Redox Potentials[a] and Comproportionation Constants for Complexes 1−4 and for the Ruthenium Analogue 5 of 1

	E°_{298}/V (ΔE_p/mV)								
compound	couple I	couple II	couple III	couple IV	couple V	K_{c1}[b]	K_{c2}[b]	K_{c3}[b]	K_{c4}[b]
5[c]	[d]	0.46(80)	−0.17(80)	−0.82(70)	−1.34(80)	[d]	$10^{10.7}$	$10^{11.0}$	$10^{8.8}$
1	0.69(107)	0.45(99)	−0.15(100)	−1.18(100)	−1.48(160)	$10^{4.1}$	$10^{10.2}$	$10^{17.5}$	$10^{5.1}$
2	0.95(130)	0.71(90)	0.12(70)	−0.92(90)	−1.22(100)	$10^{4.1}$	10^{10}	$10^{17.6}$	$10^{5.1}$
3	0.69(130)	0.48(130)	−0.11(100)	−1.15(100)	−1.45(130)	$10^{3.6}$	10^{10}	$10^{17.6}$	$10^{5.1}$
4	0.73(130)	0.55(110)	−0.0041(80)	−1.07(80)	−1.35(140)	$10^{3.1}$	$10^{10.9}$	10^{18}	$10^{4.7}$

[a] Potentials E°_{298}/V (ΔE_p/mV) versus SCE; in CH$_2$Cl$_2$/0.1 M [Et$_4$N][ClO$_4$]; scan rate, 100 mV s^{-1}. [b] $RT \ln K_c = nF(\Delta E)$. K_{c1} corresponds to couple I and couple II. K_{c2} corresponds to couple II and couple III. K_{c3} corresponds to couple III and couple IV. K_{c4} corresponds to couple IV and couple V. [c] **5** = [Ru(pap)$_2$(Q)](ClO$_4$), ref. 8; measurements in CH$_3$CN/0.1 M [Et$_4$N][ClO$_4$]. [d] Not observed, E > 0.9 V.

dx.doi.org/10.1021/ic200615s |*Inorg. Chem.* 2011, 50, 7090–7098

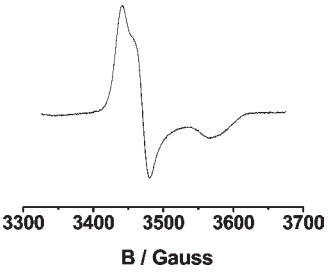

Figure 4. EPR spectrum of $\mathbf{1}^+$ at 110 K in CH_2Cl_2/0.1 M $[Bu_4N][PF_6]$.

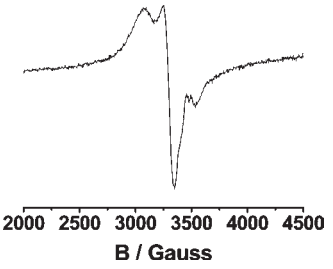

Figure 5. EPR spectrum of $\mathbf{2}^-$ at 110 K in CH_2Cl_2/0.1 M $[Bu_4N][PF_6]$.

high at about 10^{10} (Table 3). The crystal structure of one ruthenium analogue, *ctc*-$[Ru^{II}(pap^0)_2(Q^{\bullet-})](ClO_4)$ ($K_c = 10^{11}$), was reported[8] to exhibit typical[7] *o*-iminobenzosemiquinone(1-) and (pap^0) ligand structures. However, the EPR signals of the ruthenium containing cations remained unresolved at $g = 1.99$.[8] The osmium analogues with the much higher spin−orbit coupling from the 5d metal[22] proved to be more suitable for EPR analysis.

The paramagnetic cations *ctc*-$[Os^{II}(pap^0)_2(Q^{\bullet-})]^+$ ($\mathbf{1}^+$−$\mathbf{4}^+$) exhibit EPR spectra in frozen solution (Figure 4, Table 4) which are reminiscent of that of $[Os(bpy)_2(Q)]^+$ ($g_1 - g_3 = 0.370$, $\langle g \rangle = 1.960$).[23] However, at about 0.08 the g anisotropy $g_1 - g_3$ is much smaller (Table 4) for the present systems, suggesting significant participation of the π^* orbitals of the pap ligands at the spin distribution and/or less contributions from osmium. Possibly, Os→π^*(pap) back-donation diminishes the metal participation at the singly occupied molecular orbital (SOMO) in the present case. This is reproduced by DFT calculations (Supporting Information, Table S2, Figure 6); the closeness of π^*(pap) to singly occupied π^*(Q) is also evident from the $\langle g \rangle < 2$ which reflects a situation with unoccupied molecular orbitals (MOs) close to the SOMO.[24] The standard approximation for the deviation of g from g(electron) includes the spin orbit coupling constants of participating atoms as a factor and the energy differences between the SOMO and the highest occupied molecular orbitals (HOMOs) or lowest unoccupied molecular orbitals (LUMOs) in the denominator. Small SOMO/HOMO energy differences contribute to $g > 2$, and small SOMO/LUMO gaps to $g < 2$.[24]

***ctc*-Os(pap)$_2$(Q).** All four neutral compounds **1**−**4** could be structurally characterized. The high stability of these neutral compounds is also evident from K_c values of about 10^{18}. The data from Table 2 shows rather small substituent effects within the series of Scheme 1 and good reproduction by DFT calculations for the parent compound **1**.

Analysis of the structural data in comparison to statistically established values[7] reveals that the quinonoid ligands must be formulated as two-electron reduced amidophenolate dianions with

Table 4. EPR Data[a] of $\mathbf{1}^n$−$\mathbf{4}^n$

complex	g_1	g_2	g_3	Δg[b]	$\langle g \rangle$[c]
$\mathbf{1}^+$	2.013	1.995	1.935	0.078	1.981
$\mathbf{2}^+$	2.012	1.996	1.931	0.081	1.980
$\mathbf{3}^+$	2.013	1.996	1.934	0.079	1.981
$\mathbf{4}^+$	2.013	1.997	1.938	0.075	1.983
$\mathbf{2}^-$	2.253	2.099	1.958	0.295	2.107

[a] Measurements in frozen CH_2Cl_2/0.1 M $[Bu_4N][PF_6]$ at 110 K. [b] $\Delta g = g_1 - g_3$. [c] $\langle g \rangle = [(g_1^2 + g_2^2 + g_3^2)/3]^{1/2}$.

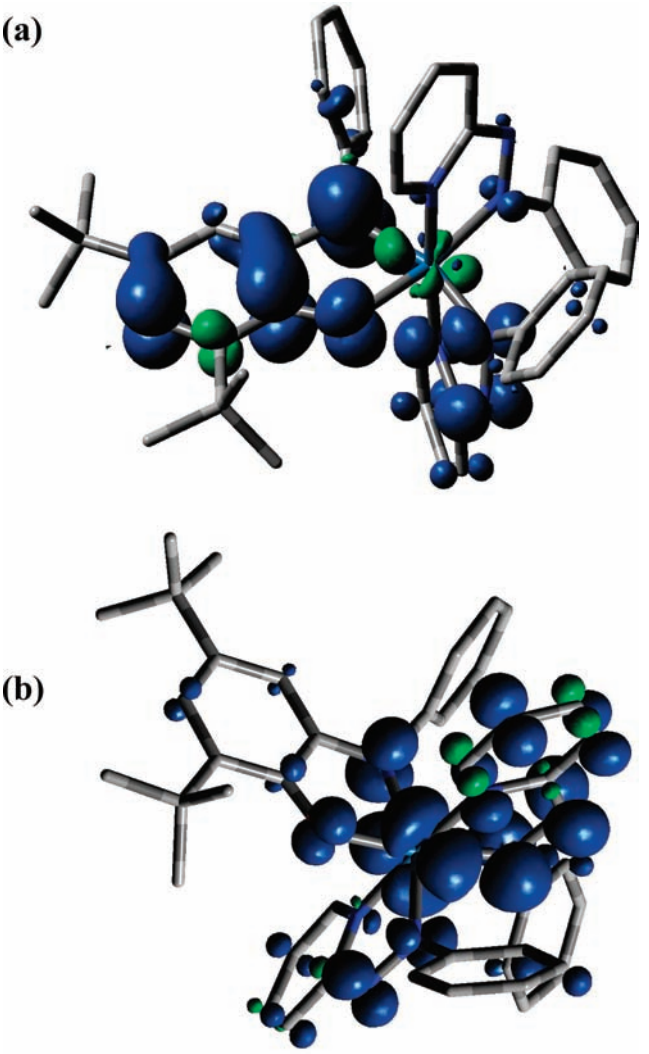

Figure 6. Spin density representations of (a) $\mathbf{1}^+$ and (b) $\mathbf{1}^-$.

aromatic rings and C−O and C−N exocyclic single bonds. While this result is not unexpected,[8] the inspection of the two pap ligands with their N−N distances of about 1.33 Å points clearly to the established anion character of these ligands because neutral pap and similar ligands have d(N−N) < 1.30 Å, even when π back-donation from the metal is present.[5,6,8,21] This would leave an osmium(IV) oxidation state on the metal, in contrast to the metal(II) formulation with unreduced pap postulated for the ruthenium analogues.[8]

dx.doi.org/10.1021/ic200615s |*Inorg. Chem.* 2011, 50, 7090–7098

DFT calculations reproduce the observed invariant structures for the neutral configuration rather well (Table 2). They also lend support to the *ctc*-$Os^{IV}(pap^{\bullet-})_2(Q^{2-})$ assignment because Table 7 identifies the HOMO as a $Q^{2-}/pap^{\bullet-}$ MO combination while the LUMO is a $pap^{\bullet-}/Os^{IV}$ mixed MO (Figure 7). Experimental evidence for this formulation comes from the notable shortening of bonds by 0.03−0.06 Å between osmium and the coordinating N atoms of pap when going from the dication (pap^0 ligands) to the neutral forms $pap^{\bullet-}$ (Table 2). The ^1H NMR spectra do not show any paramagnetic shifts (see Experimental Section) or undue line-broadening which agrees with the calculated large separation of 1955 cm^{-1} between the singlet ground state of **1** and the next triplet state. The unpaired electrons formally implied in the representation *ctc*-$Os^{IV}(pap^{\bullet-})_2(Q^{2-})$ are apparently strongly coupled with the effect of complete spin pairing. It must be conceded, however, that the apparent covalency in the bonding between metal and ligands allows for the reasonable inclusion of other oxidation state combinations (see Scheme 2) with various degrees of plausibility.

***ctc*-[Os(pap)$_2$(Q)]$^-$.** Reduction of the neutral compounds yields anions with typical K_c values of 10^5 (Table 3). In the absence of experimental structure data, the EPR spectrum obtained for $\mathbf{2}^-$ (Figure 5, Table 4) serves to evaluate the most appropriate oxidation state formulation. The intermediate *g* factor anisotropy of $g_1 - g_3 = 0.295$ is neither compatible with an unfettered Os^{III} configuration (e.g., $g_x = 2.836$, $g_y = 2.535$, $g_z = 1.400$ for $[Os^{III}(Me\text{-}xanthate)(PPh_3)_2]^+$)[25] nor with a typical osmium-modified

Table 5. UV−vis−NIR Data for $\mathbf{1}^n$−$\mathbf{4}^n$ in Various Oxidation States from OTTLE Spectroelectrochemistry in CH_2Cl_2/0.1 M $[Bu_4N][PF_6]$

compound	λ/nm (ε/M^{-1} cm^{-1})
$\mathbf{1}^{2+}$	740sh, 608(8800), 550(10000), 513(11000), 392(10800), 330(12100), 275sh
$\mathbf{1}^{+}$	1645(950), 795sh, 694(5300), 557(5600), 478(7000), 390sh, 338(15400), 284(20600)
1	1370(1700), 923(5200), 530sh, 461(6500), 333(16900), 285(20200), 240(24000)
$\mathbf{1}^{-}$	1575br, 1425sh, 837(3600), 645sh, 594(3200), 470sh, 430(9500), 313sh, 282(21700)
$\mathbf{2}^{2+}$	730sh, 617(7200), 507(7500), 392(8700), 338(9700), 284(15100)
$\mathbf{2}^{+}$	1575br, 790sh, 702(4600), 560(4300), 478(5500), 390sh, 345(11700), 285(16200)
2	1365(1200), 896(4070), 530sh, 467(5200), 330sh, 287(16800)
$\mathbf{2}^{-}$	1650sh, 796(2600), 660sh, 589(3000), 455sh, 400(9200), 305(20400)
$\mathbf{3}^{2+}$	730sh, 610(8300), 510(8700), 390sh, 327(10100), 270(14500)
$\mathbf{3}^{+}$	1624(960), 1035sh, 790sh, 695(4600), 560sh, 478(5900), 400sh, 320(12400), 280sh
3	1395(1500), 922(4500), 527(4000), 460(5600), 335(13800), 285sh
$\mathbf{3}^{-}$	1760(600), 1395sh, 834(3000), 610(2900), 470sh, 400(8100), 308(15300)
$\mathbf{4}^{2+}$	755sh, 566sh, 530(13600), 400sh, 330(11100), 265(19300)
$\mathbf{4}^{+}$	1675(945), 980sh, 785(2900), 685(4100), 555sh, 485(6000), 390sh, 330sh, 285(17600)
4	1385(1530), 955(4550), 525(4100), 460(5700), 330(14700), 285(18900)
$\mathbf{4}^{-}$	1630(725), 850(3000), 610(2700), 450sh, 390sh, 287(20100)

Table 7. Energies and Compositions of Selected Molecular Orbitals for 1 in the Singlet Ground State

		composition		
MO	energy/eV	Os	pap	Q
LUMO+5	−0.38	04	38	58
LUMO+4	−0.47	01	66	33
LUMO+3	−0.94	03	96	01
LUMO+2	−1.25	04	96	0
LUMO+1	−2.38	25	63(N═N, 25)	12
LUMO	−2.81	23	58(N═N, 31)	19
HOMO	−4.17	03	41(N═N, 20)	56
HOMO−1	−5.16	30	06	64
HOMO−2	−5.80	31	55(N═N, 23)	14
HOMO−3	−5.96	46	28	26
HOMO−4	−6.11	41	13	46
HOMO−5	−6.58	06	68	26
HOMO−6	−6.59	01	39	60
HOMO−7	−6.83	03	90	07
HOMO−8	−6.88	01	90	09
HOMO−9	−6.86	01	24	75
HOMO−10	−6.92	01	81	18

Table 6. TD-DFT Calculated Electronic Transitions of 1

energy/eV	λ/nm	*f*	transition	character
0.872	1421	0.0148	(62%)HOMO → LUMO	pap(π)/Q(π) → pap(π^*)
1.326	935	0.0287	(70%)HOMO−1 → LUMO	Os(dπ)/Q(π) → pap(π^*)
1.360	912	0.0596	(55%)HOMO−1 → LUMO+1	Os(dπ)/Q(π) → pap(π^*)
2.267	547	0.0331	(41%)HOMO−4 → LUMO	Os(dπ)/Q(π) → pap(π^*)
			(29%)HOMO−3 → LUMO	Os(dπ) → pap(π^*)
2.391	519	0.0104	(42%)HOMO−5 → LUMO	pap(π) → pap(π^*)
			(25%)HOMO−3 → LUMO	Os(dπ) → pap(π^*)
2.562	484	0.0359	(41%)HOMO−5 → LUMO	pap(π) → pap(π^*)
			(29%)HOMO−4 → LUMO	Os(dπ)/Q(π) → pap(π^*)
2.729	454	0.0633	(57%)HOMO−5 → LUMO+1	pap(π) → pap(π^*)
			(25%)HOMO−4 → LUMO+1	Os(dπ)/Q(π) → pap(π^*)

dx.doi.org/10.1021/ic200615s |*Inorg. Chem.* 2011, 50, 7090–7098

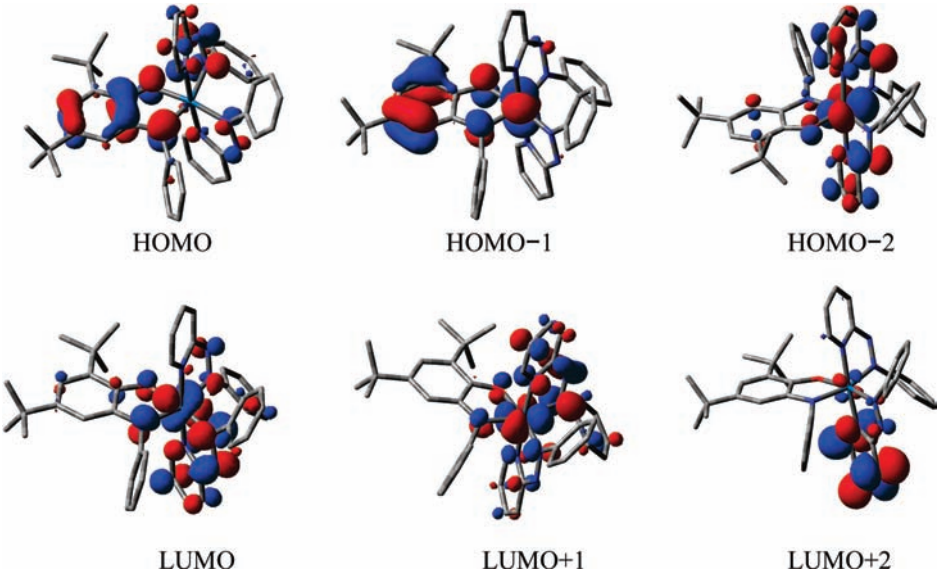

Figure 7. Representative orbital contour diagrams of **1**.

Scheme 2

$[Os^{II}(pap^0)_2(Q^0)]^{2+}$ or $[Os^{III}(pap^0)_2(Q^{\bullet -})]^{2+}$

$-e^- \rightleftharpoons +e^-$

$[Os^{II}(pap^0)_2(Q^{\bullet -})]^{+}$

$-e^- \rightleftharpoons +e^-$

$[Os^{IV}(pap^{\bullet -})_2(Q^{2-})]$ or $[Os^{III}(pap^{\bullet -})_2(Q^{\bullet -})]$

$-e^- \rightleftharpoons +e^-$

$[Os^{II}(pap^0)(pap^{\bullet -})(Q^{2-})]^{-}$ or $[Os^{III}(pap^{\bullet -})_2(Q^{2-})]^{-}$

organic radical.[26] That leaves both plausible alternatives *ctc*-$[Os^{III}(pap^{\bullet -})_2(Q^{2-})]^{-}$ and *ctc*-$[Os^{II}(pap^{\bullet -})(pap^0)(Q^{2-})]^{-}$ as possibilities within a resonance situation; the formation of pap^{2-} is not likely due to the loss of aromatic stabilization. DFT calculations favor the latter alternative with Mulliken spin densities of 0.315 (Os), 0.579 ($pap^{\bullet -}$), 0.067 (pap^0), and 0.039 (Q^{2-}) in $\mathbf{1}^{-}$; however, the situation involves considerable covalency. The larger *g* anisotropy for the anion in comparison to the cation would then be attributed to higher spin polarization from the pap radical anion to the metal while the higher *g* values ($g > 2$) reflect the closeness of the filled π^* MO of Q^{2-} relative to the SOMO.[24] As outlined above, the standard approximation for the deviation of *g* from *g*(electron) includes the spin orbit coupling constants of participating atoms as a factor and the energy differences between the SOMO and the HOMOs or LUMOs in the denominator. Small SOMO/HOMO energy differences contribute to $g > 2$, and small SOMO/LUMO gaps to $g < 2$.

UV−vis−NIR Spectroelectrochemistry. On the basis of the oxidation state formulations delineated above, the results from electronic absorption spectroscopy via OTTLE cell spectroelectrochemistry can be discussed (Supporting Information, Figures S5−S10, Table 5) and understood using TD-DFT calculation results (Table 6, Supporting Information, Tables S6−S8).

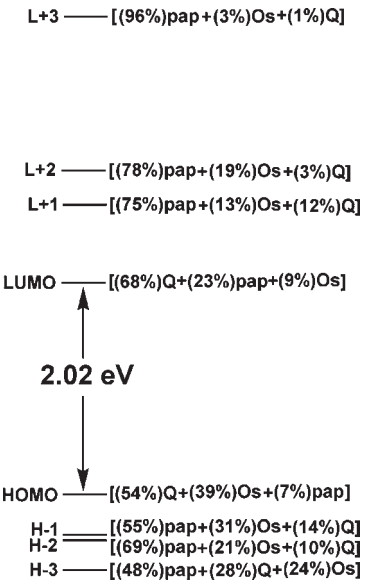

Figure 8. Orbital energy diagram for $\mathbf{1}^{2+}$.

In agreement with a large HOMO−LUMO gap (Figure 8) the dications $\mathbf{1}^{2+}$−$\mathbf{4}^{2+}$ exhibit absorptions in the visible which can be described as MLCT/LL′CT with the empty π^* orbitals of Q or pap as targets of the transitions (Supporting Information, Table S7 and Figures S5, S8−S10). On reduction by one-electron the resulting iminosemiquinone complexes show weak absorption in the near-infrared region (ca. 1600 nm, Supporting Information, Figures S6, S8−S10, Table 5). Corresponding interligand charge transfer (LL′CT) transitions were calculated by TD-DFT procedures (Supporting Information, Table S6). The neutral forms with the structurally established unusual oxidation state configuration *ctc*-$Os^{IV}(pap^{\bullet -})_2(Q^{2-})$ have also

dx.doi.org/10.1021/ic200615s |*Inorg. Chem.* 2011, 50, 7090–7098

NIR absorption bands of intermediate intensity around 1370 nm (Supporting Information, Figures S6−S10, Table 5), assigned to interligand charge transfer transitions and followed by mixed MLCT/LL′CT transitions in the NIR and vis regions (Table 6). Finally, the anions exhibit weak shoulders around 1600 nm (Supporting Information Figures S7−S10, Table 5) based on transitions from the occupied Q^{2-} or $pap^{\bullet-}$ ligand orbitals to the π^* level of unreduced pap (Supporting Information, Table S8).

4. CONCLUDING REMARKS

The complete analysis of the four-component redox series studied here was possible through a combination of various techniques, especially multiple structural data and EPR information in conjunction with DFT calculations. The results are consistent, show little substituent effects, and are illustrated by Scheme 2, and they reveal a few remarkable features: The 3-fold oxidation state change on going from the cations *ctc*-$[Os^{II}(pap)_2(Q^{\bullet-})]^+$ to the neutral forms *ctc*-$Os^{IV}(pap^{\bullet-})_2(Q^{2-})$ indicates a complex example of "redox-induced electron transfer" (RIET)[27] which has been somewhat relatedly observed for other osmium (II,III, IV) complexes.[28] The strong σ and π donating capacity of reductively formed catecholates[29] and related systems[30] favors the higher, here the metal(IV), oxidation state, also in relation to the lighter homologue, ruthenium.[8] This amidophenolate-induced donor effect seems to be the trigger for the RIET behavior between osmium and two pap ligands. Further reduction restores the low metal oxidation state and results in different spin densities on the two pap ligands in *ctc*-$[Os^{II}(pap^{\bullet-})(pap^{0})(Q^{2-})]^-$, with only minor contributions from the osmium(III) alternative *ctc*-$[Os^{III}(pap^{\bullet-})_2(Q^{2-})]^-$. Both experimental and computational studies reveal considerable metal/ligand orbital mixing (covalency) which is reflected by the small substituent effects.

The behavior of the redox potentials and the comproportionation constants K_c (Table 3) invite a discussion and comparison with the ruthenium analogues.[8] While the Q-based redox reactions (couples II, III from Table 3) show identical potentials, the other, more metal-involving processes exhibit cathodic shifts for the osmium systems. As a result of the thus facilitated oxidation but disfavored reduction of the osmium analogues the comproportionation constants for some intermediates can be distinctly different. Specifically, the neutral forms presented here are stabilized relative to the Ru analogues, while the paramagnetic cation and anion states exhibit lower stability (Table 3). It is thus of crucial importance to correctly assess the proper oxidation state combination to evaluate the range of existence and reactivity potential, the present case revealing remarkable differences as well as similarities between analogous ruthenium[8] and osmium systems.

■ ASSOCIATED CONTENT

Supporting Information. X-ray crystallographic files in CIF format for **1**, **2**, **3**, **4**, and $(\mathbf{3})(ClO_4)_2$, molecular structure representations of **2**, **3**, and **4** (Figures S1−S3), table of experimental and calculated bond angles (Table S1), DFT data set for **1** (Tables S2−S8 and Figure S4), spectroelectrochemistry figures for $\mathbf{1}^m$ (Figures S5−S7), $\mathbf{2}^m$ (Figure S8), $\mathbf{3}^m$ (Figure S9) and $\mathbf{4}^m$ (Figure S10). This material is available free of charge via the Internet at http://pubs.acs.org.

■ AUTHOR INFORMATION

Corresponding Author

*E-mail: kaim@iac.uni-stuttgart.de (W.K.), lahiri@chem.iitb.ac.in (G.K.L.). Phone: +49(0)711/685-64170 (W.K.), +91 22 25767159 (G.K.L.). Fax: +49(0)711/685−64165 (W.K.), +91 22 25723480 (G.K.L.).

■ ACKNOWLEDGMENT

Financial support received from the Department of Science and Technology and University Grant commission (New Delhi, India), from the DAAD and the DFG, the Grant Agency of the Czech Republic (Grant 203/09/0705) is gratefully acknowledged. X-ray structural studies for **1**−**4** and $(\mathbf{3})(ClO_4)_2$ were carried out at the National Single Crystal Diffractometer Facility, Indian Institute of Technology Bombay. ^1H NMR experiments were carried out at the Sophisticated Analytical Instrument Facility (SAIF), Indian Institute Technology Bombay.

■ REFERENCES

(1) Kaim, W., accepted FORUM contribution to *Inorg. Chem.*, (ic-2011-003832).

(2) Kaim, W.; Schwederski, B. *Coord. Chem. Rev.* **2010**, *254*, 1580.

(3) (a) Das, A. K.; Sarkar, B.; Duboc, C.; Strobel, S.; Fiedler, J.; Zalis, S.; Lahiri, G. K.; Kaim, W. *Angew. Chem., Int. Ed.* **2009**, *48*, 4242. (b) Singh, P.; Das, A. K.; Sarkar, B.; Niemeyer, M.; Roncaroli, F.; Olabe, J. A.; Fiedler, J.; Zalis, S.; Kaim, W. *Inorg. Chem.* **2008**, *47*, 7106.

(4) Poddel'sky, A. I.; Cherkasov, V. K.; Abakumov, G. A. *Coord. Chem. Rev.* **2009**, *253*, 291.

(5) (a) Pramanik, K.; Shivakumar, M.; Ghosh, P.; Chakravorty, A. *Inorg. Chem.* **2000**, *39*, 195. (b) Goswami, S.; Chakravarty, A. R.; Chakravorty, A. *Inorg. Chem.* **1981**, *20*, 2246. (c) Ghosh, B. K.; Mukhopadhyay, A.; Goswami, S.; Ray, S.; Chakravarty, A. R.; Chakravorty, A. *Inorg. Chem.* **1984**, *23*, 4633. (d) Ghumaan, S.; Mukherjee, S.; Kar, S.; Roy, D.; Shaikh, M. M.; Sunoj, R. B.; Lahiri, G. K. *Eur. J. Inorg. Chem.* **2006**, 4426. (e) Das, C.; Peng, S.-M.; Leeb, G.-H.; Goswami, S. *New J. Chem.* **2002**, *26*, 222.

(6) (a) Hartmann, H.; Scheiring, T.; Fiedler, J.; Kaim, W. *J. Organomet. Chem.* **2000**, *604*, 267. (b) Frantz, S.; Hartmann, H.; Doslik, N.; Wanner, M.; Kaim, W.; Kümmerer, H.-J.; Denninger, G.; Barra, A.-L.; Duboc-Toia, C.; Fiedler, J.; Ciofini, I.; Urban, C.; Kaupp, M. *J. Am. Chem. Soc.* **2002**, *124*, 10563. (c) Sarkar, B.; Patra, S.; Fiedler, J.; Sunoj, R. B.; Janardanan, D.; Mobin, S. M.; Niemeyer, M.; Lahiri, G. K.; Kaim, W. *Angew. Chem., Int. Ed.* **2005**, *44*, 5655. (d) Sarkar, B.; Patra, S.; Fiedler, J.; Sunoj, R. B.; Janardanan, D.; Lahiri, G. K.; Kaim, W. *J. Am. Chem. Soc.* **2008**, *130*, 3532.

(7) Bhattacharya, S.; Gupta, P.; Basuli, F.; Pierpont, C. G. *Inorg. Chem.* **2002**, *41*, 5810.

(8) Das, D.; Mondal, T. K.; Mobin, S. M.; Lahiri, G. K. *Inorg. Chem.* **2009**, *48*, 9800.

(9) Ghosh, B. K.; Goswami, S.; Chakravorty, A. *Inorg. Chem.* **1983**, *22*, 3358.

(10) (a) Chaudhuri, P.; Verani, C. N.; Bill, E.; Bothe, E.; Weyhermüller, T.; Wieghardt, K. *J. Am. Chem. Soc.* **2001**, *123*, 2213. (b) Mukherjee, S.; Weyhermüller, T.; Bothe, E.; Wieghardt, K.; Chaudhuri, P. *Dalton Trans.* **2004**, 3842.

(11) Krejcik, M.; Danek, M.; Hartl, F. *J. Electroanal. Chem.* **1991**, *317*, 179.

(12) Kaim, W.; Ernst, S.; Kasack, V. *J. Am. Chem. Soc.* **1990**, *112*, 173.

(13) Sheldrick, G. M. *SHELX-97, Program for Crystal Structure Solution and Refinement*; University of Göttingen: Göttingen, Germany, 1997.

(14) Lee, C.; Yang, W.; Parr, R. G. *Phys. Rev. B* **1988**, *37*, 785.

(15) (a) Andrae, D.; Haeussermann, U.; Dolg, M.; Stoll, H.; Preuss, H. *Theor. Chim. Acta* **1990**, *77*, 123. (b) Fuentealba, P.; Preuss, H.; Stoll, H.; von Szentpaly, L. *Chem. Phys. Lett.* **1989**, *89*, 418.

(16) Frisch, M. J. et al. *Gaussian 03*; Gaussian, Inc.: Wallingford, CT, 2004.

(17) (a) Bauernschmitt, R.; Ahlrichs, R. *Chem. Phys. Lett.* **1996**, *256*, 454. (b) Stratmann, R. E.; Scuseria, G. E.; Frisch, M. J. *J. Chem. Phys.* **1998**, *109*, 8218. (c) Casida, M. E.; Jamorski, C.; Casida, K. C.; Salahub, D. R. *J. Chem. Phys.* **1998**, *108*, 4439.

(18) (a) Barone, V.; Cossi, M. *J. Phys. Chem. A* **1998**, *102*, 1995. (b) Cossi, M.; Barone, V. *J. Chem. Phys.* **2001**, *115*, 4708. (c) Cossi, M.; Rega, N.; Scalmani, G.; Barone, V. *J. Comput. Chem.* **2003**, *24*, 669.

(19) O'Boyle, N. M.; Tenderholt, A. L.; Langner, K. M. *J. Comput. Chem.* **2008**, *29*, 839.

(20) Lay, P. A.; Magnuson, R. H.; Taube, H. *Inorg. Chem.* **1988**, *27*, 2364.

(21) Kaim, W.; Kohlmann, S.; Jordanov, J.; Fenske, D. *Z. Anorg. Allg. Chem.* **1991**, *598/599*, 217.

(22) Kober, E. M.; Meyer, T. J. *Inorg. Chem.* **1983**, *22*, 1614.

(23) Ye, S.; Sarkar, B.; Duboc, C.; Fiedler, J.; Kaim, W. *Inorg. Chem.* **2005**, *44*, 2843.

(24) Kaim, W. *Coord. Chem. Rev.* **1987**, *76*, 187.

(25) Pramanik, A.; Bag, N.; Ray, D.; Lahiri, G. K.; Chakravorty, A. *Inorg. Chem.* **1991**, *30*, 410.

(26) (a) Baumann, F.; Kaim, W.; Denninger, G.; Kümmerer, H.-J.; Fiedler, J. *Organometallics* **2005**, *24*, 1966. (b) Heilmann, M.; Frantz, S.; Kaim, W.; Fiedler, J.; Duboc, J. *Inorg. Chim. Acta* **2006**, *359*, 827.

(27) Miller, J. S.; Min, K. S. *Angew. Chem.* **2009**, *121*, 268. *Angew. Chem., Int. Ed.* **2009**, *48*, 262.

(28) Samanta, S.; Singh, P.; Fiedler, J.; Zalis, S.; Kaim, W.; Goswami, S. *Inorg. Chem.* **2008**, *47*, 1625.

(29) Darensbourg, D. J.; Klausmeyer, K. K.; Reibenspies, J. H. *Inorg. Chem.* **1996**, *35*, 1529.

(30) (a) Berger, S.; Baumann, F.; Scheiring, T.; Kaim, W. *Z. Anorg. Allg. Chem.* **2001**, *627*, 620. (b) Kaim, W.; Sieger, M.; Greulich, S.; Sarkar, B.; Fiedler, J.; Zalis, S. *J. Organomet. Chem.* **2010**, *695*, 1052.